

The room temperature prodrome of charge-order in copper oxides

S. Peli,^{1,2} S. Dal Conte,³ R. Comin,^{4,5} N. Nembrini,^{1,2} F. Banfi,^{1,6} G. Ferrini,^{1,6} D. Brida,⁷
S. Lupi,⁸ M. Fabrizio,⁹ M. Capone,⁹ A. Damascelli,^{4,5} G. Cerullo,³ and C. Giannetti^{1,6}

¹*Department of Physics, Università Cattolica del Sacro Cuore, Brescia I-25121, Italy*

²*Department of Physics, Università degli Studi di Milano, Italy*

³*IFN-CNR, Dipartimento di Fisica, Politecnico di Milano, 20133 Milano, Italy*

⁴*Quantum Matter Institute, University of British Columbia, Vancouver, BC V6T 1Z4, Canada*

⁵*Department of Physics and Astronomy, University of British Columbia, Vancouver, BC V6T 1Z1, Canada*

⁶*i-LAMP (Interdisciplinary Laboratories for Advanced Materials Physics),*

Università Cattolica del Sacro Cuore, Brescia I-25121, Italy

⁷*Department of Physics and Center for Applied Photonics,*

University of Konstanz, 78457 Konstanz, Germany

⁸*CNR-IOM Dipartimento di Fisica, Università di Roma La Sapienza P.le Aldo Moro 2, 00185 Rome, Italy*

⁹*Scuola Internazionale Superiore di Studi Avanzati (SISSA) and CNR-IOM*

Democritos National Simulation Center, Via Bonomea 265, 34136 Trieste (Italy)

An intrinsic instability towards inhomogeneous states is emerging as the prominent feature of underdoped cuprates and manifests itself in a variety of ways including the spontaneous emergence of charge-order patterns at low temperature. The experimental evidences show a general trend where various instabilities, that break different symmetries at the nanometric scale, appear below a characteristic temperature and only up to a critical hole doping p_{cr} . This revives the long debated question whether this behaviour is just the consequence of the tendency to develop a specific long-range symmetry-broken phase, or it is the low-energy manifestation of a more general precursory state, which arises from strong electronic correlations suddenly changing at p_{cr} . Here we solve this question by investigating the ultrafast dynamics of the O-2p→Cu-3d charge-transfer process in Bi₂Sr_{2-x}La_xCuO_{6+δ}, and by linking these results to the doping evolution of the charge-order instability on the same material. We demonstrate that the doping p_{cr} , at which the amplitude of the spontaneous charge modulation vanishes at low temperature, also marks a sharp and drastic change in the character of the Cu-3d and O-2p wavefunctions, that turn from localized –as in a Mott insulator– to delocalized –as in a conventional metal. Since the $p=p_{cr}$ turning point is observed at room temperature, we conclude that there exists an underlying correlated state, characterized by the localization of the Cu-O wavefunctions and the related quenching of the O-2p→Cu-3d charge fluctuations, that is precursor to the low-temperature charge-order and, possibly, to the other instabilities that fan out from a zero-temperature quantum critical point at p_{cr} .

The origin of the low-temperature fragility of underdoped cuprates towards a wealth of different symmetry-breaking instabilities is presently one of the most debated issues in the physics of correlated materials. The breaking of the rotational symmetry from C_4 to C_2 (nematicity) has been argued from X-ray and neutron scattering experiments[1–3] and directly imaged by scanning tunneling microscopy (STM)[4]. The signature of intra-unit-cell magnetic order has been observed by neutron scattering[5] and Kerr effect measurements[6]. More recently, the universal tendency to develop short-ranged incommensurate charge density waves (CDW) that break the translational symmetry has been reported in both hole- and electron-doped copper oxides[7–15].

Many efforts have been directed to unveil the mechanisms underlying this complex phenomenology. An experimental step forward has been the observation[16, 17] that at $T \simeq 0$ the breaking of the electronic symmetries is accompanied by a simultaneous transition in the momentum space topology, which can be ascribed either to a nematic transition involving the oxygens within the CuO₂ unit cell[16] or to a CDW-driven reconstruction of the Brillouin zone. Theoretically, it has been recently shown[18–22] that electron-electron interactions mediated by the spin fluctuations can give rise to a charge order instability with the correct wavevector[10] and also the experimentally-observed d -wave symmetry[23, 24]. The same mechanism can induce an instability towards composite CDW orders[18, 25] that break time-reversal and C_4 rotational symmetry.

All these recent results raise fundamental questions about the hierarchy of the different instabilities and the possible existence of a common origin, which might nestle within the intrinsic properties of the CuO₂ plane. On a general level, the tendency to develop charge-order stems from the competition between the optimization of the kinetic energy and the minimization of the Coulomb repulsion related to the charge and lattice inhomogeneities. Among the different ingredients, whose interplay leads to specific instabilities in different compounds, the presence of strong short-range Coulomb interactions between the charges within the CuO₂ unit cell is a common feature to all underdoped copper

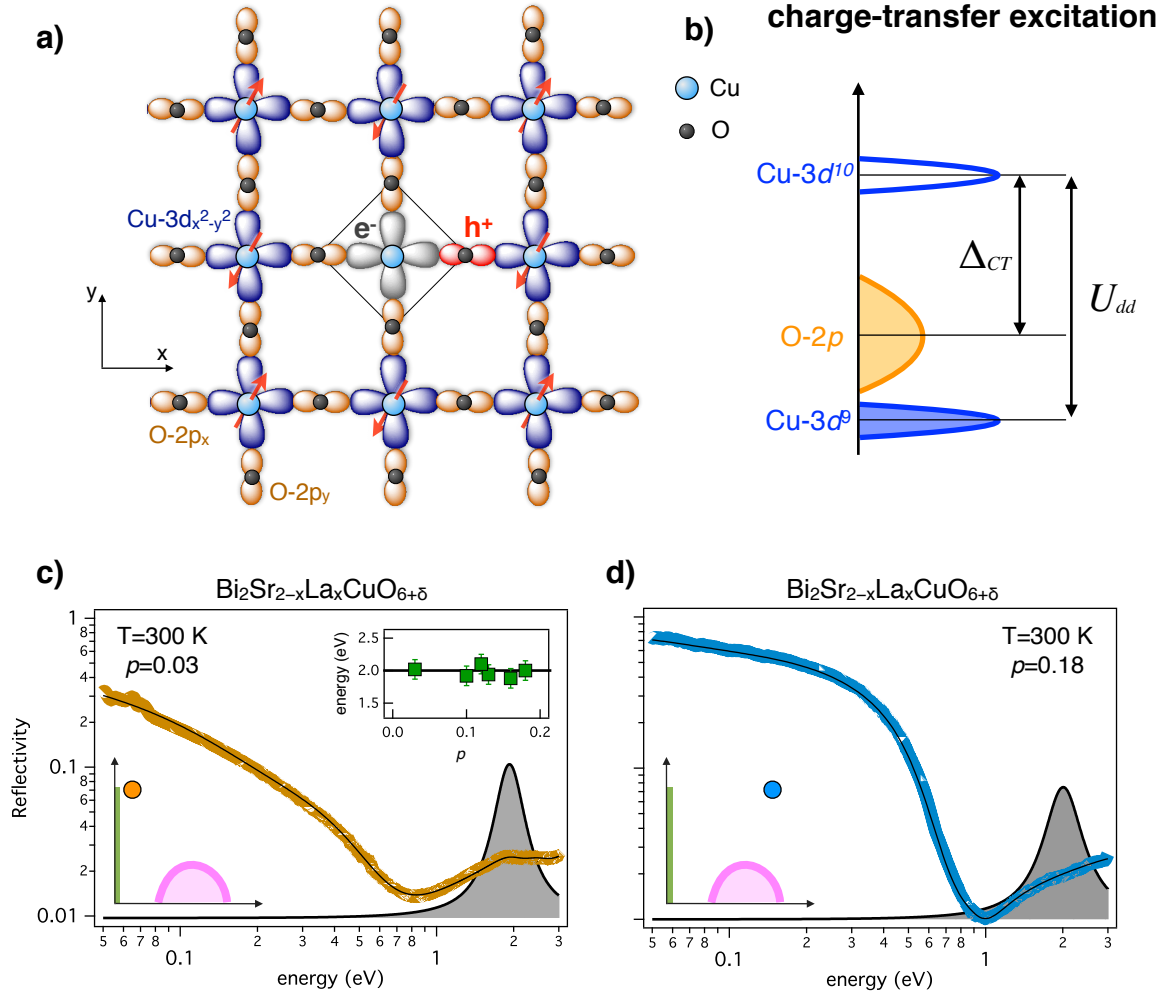


FIG. 1: Charge-transfer excitation and optical properties of cuprates. a,b) A sketch of the generic charge-transfer process in the Cu-O layer of copper oxides is shown. **c)** The reflectivity curve, $R(\omega)$ of the underdoped sample is reported (yellow dots). The black line is the fit to the data obtained from a model dielectric function which contains an extended-Drude term and three Lorentz oscillators that account for the high-energy transitions. The contribution of the first interband oscillator (ω_{CT}), attributed to the charge-transfer process, to the total dielectric function is reported as a grey region. The inset displays ω_{CT} as a function of the hole concentration. The left-bottom inset shows the position of the sample in the p - T phase diagram. The pink line represents the superconducting dome, while the green line indicates the CT insulating region. **d)** The panel displays the $R(\omega)$ of the overdoped sample (blue dots). The black line is the fit of the model dielectric function to the data. The grey area represents the contribution of the CT oscillator to the dielectric function. The left-bottom inset shows the position of the sample in the p - T phase diagram.

oxides. Considering the simplest case of the parent insulator ($p=0$), the valence fluctuations of Cu-3d⁹ are suppressed by the strong Coulomb repulsion ($U_{dd} \sim 10$ eV) between two electrons occupying the same Cu orbital. The lowest excitation is thus the charge-transfer (CT) of a localized Cu-3d _{x^2-y^2} hole to its neighbouring O-2p _{x,y} orbitals (see Fig. 1a,b), with an energy cost $\Delta_{CT} \sim 2$ eV $<$ U_{dd} . In the optical conductivity, this process is revealed by a typical charge-transfer (CT) edge at $\hbar\omega = \Delta_{CT}$, which defines the onset of optical absorption by particle-hole excitations in the complete absence of a Drude response[26]. Since conventional spectroscopic techniques probe the physical properties at equilibrium, in which only the fluctuations at the energy scale $k_B T \ll \Delta_{CT}$ are thermally activated, the relation between the character of the CT process, which is related to the short-range Coulomb interactions, and the low-temperature onset of symmetry-breaking instabilities has remained hitherto unexplored.

Here we adopt a non-equilibrium approach based on the use of ultrashort light pulses to provide the photoexcited particle-hole pairs with an energy much larger than $k_B T$. The high temporal resolution (~ 10 fs) of the experiment allows us to access the dynamics of the high-energy electronic excitations before the complete thermalization is achieved. We apply this technique to the single-layer $\text{Bi}_2\text{Sr}_{2-x}\text{La}_x\text{CuO}_{6+\delta}$ (La-Bi2201) cuprate family (see Methods),

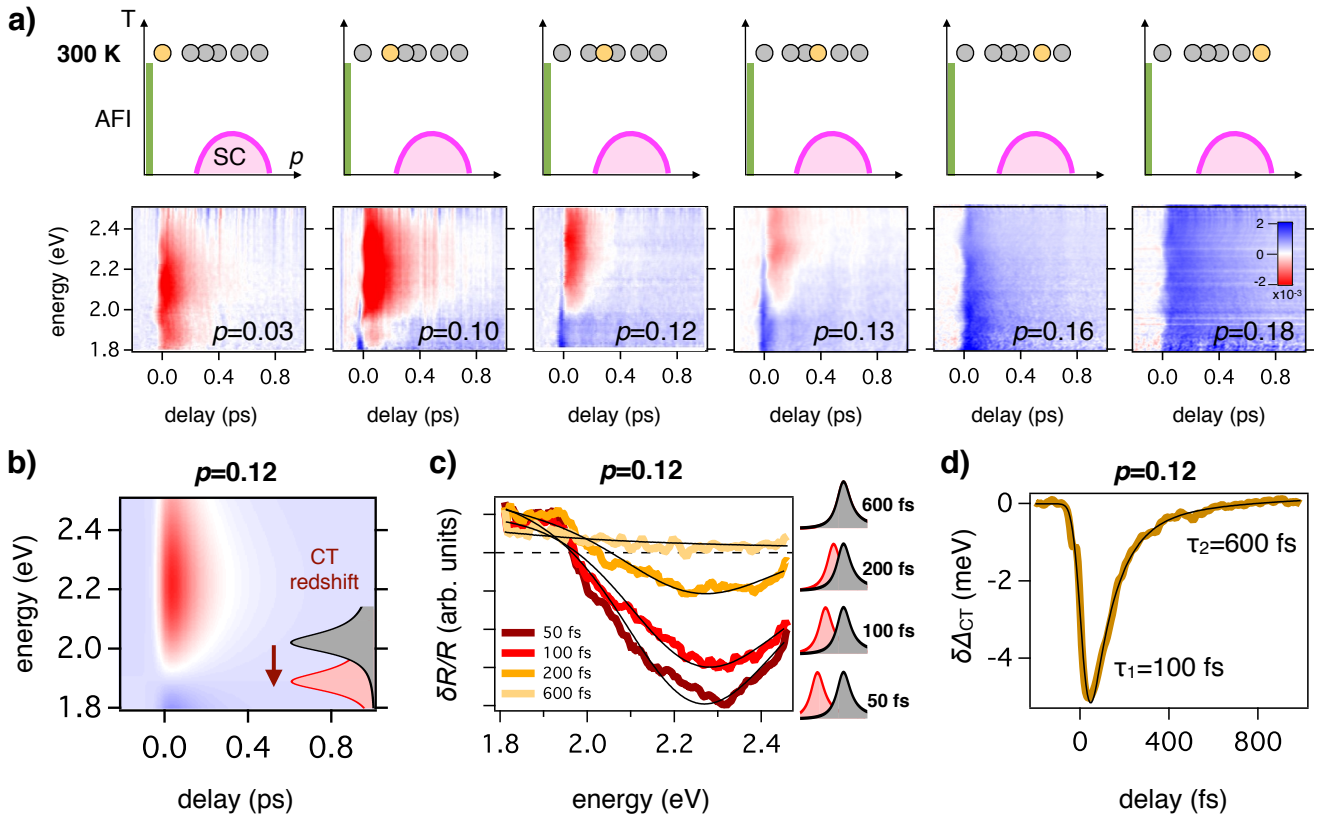


FIG. 2: **Ultrafast optical spectroscopy on La-Bi2201.** **a)** The top row shows the position of the measured samples in the p - T phase diagram. In the bottom row we report the $\delta R(\omega, t)/R$ matrices measured by ultrafast optical spectroscopy on La-Bi2201. The colour scale is reported in the inset. **b)** Simulation of the $\delta R(\omega, t)/R$ signal for the $p=0.12$ sample. A transient redshift of the CT oscillator, described by an exponential decay, is assumed. The colour scale is the same than that in panel a). **c)** Frequency-traces at different time delays for the $p=0.12$ sample. The black line is the fit to the data obtained by modifying the position of the CT oscillator. **d)** Dynamics of $\delta\Delta_{CT}$ for the $p=0.12$ sample. The black line is the fit to the data of a double-exponential decay convoluted with a step function.

in which the hole doping concentration can be accurately controlled by La substitution and can span a broad doping region ($0.03 < p < 0.18$) across the critical doping ($p_{cr} \sim 0.16$) at which the instabilities seem to vanish. The ultrafast dynamics of the CT excitation is directly compared to the CDW amplitude, that has been measured on the same samples by resonant soft X-ray scattering (RXS) at low temperature[10]. These results clarify the relation between the nature of the $O-2p \rightarrow Cu-3d$ charge fluctuations and the low-temperature charge-ordering phenomenon.

In Figure 1c,d we report the reflectivity curves, $R(\omega)$, for the most underdoped ($p=0.03$, non-superconducting) and the most overdoped ($p=0.18$, $T_c/T_{c,max}=0.57$) samples[27, 28]. Considering the deeply underdoped sample, the first high-energy optical transition is found at $\Delta_{CT}=2$ eV and hence can be safely ascribed to the charge-transfer process. When the doping concentration is increased, the energy of this optical transition remains constant (see the inset of Fig. 1c), while its spectral weight progressively decreases. Furthermore, the low-energy region develops a pronounced metallic plasma edge at $\hbar\omega \sim 1$ eV.

Fig. 2a reports the ultrafast dynamics of the CT transition at $T=300$ K in the 1.8-2.5 eV energy range, after the excitation with a sub-10 fs pulse centered at 1.4 eV. Similar results were obtained with 1.5 eV and 3 eV pump photon energies, thus demonstrating that the pumping process is non-selective and ultimately triggers the creation of a out-of-equilibrium distribution of electron-hole excitations at the CT energy. When focusing on the sub-ps

dynamics, the data exhibit a clear doping dependence. While the reflectivity variation ($\delta R(\omega)/R$) measured on the underdoped samples is characterized by a pronounced negative (red) band for $\hbar\omega > 2$ eV, it progressively evolves toward a featureless positive (blue) signal for $p > 0.16$.

The negative $\delta R(\omega)/R$ measured in underdoped samples at $\hbar\omega \sim \Delta_{CT}$ cannot be explained by assuming the simple variation of the total scattering of the charge carriers in the conduction band[29, 30], since this would lead to a featureless and positive signal over the entire probed frequency range (see Supplementary). In contrast, the $\delta R(\omega)/R$ signal can be perfectly reproduced by assuming a pump-induced redshift of the CT transition (see Supplementary), which results in a reflectivity variation proportional to the derivative of the peak shape. In Fig. 2b we report the $\delta R(\omega, t)/R$ signal calculated by introducing a redshift of the CT transition in the equilibrium dielectric function of the intermediately doped sample ($p=0.12$) and by assuming an exponential decay of the signal. The main features of the experimental transient reflectivity map are qualitatively reproduced by this simple assumption. For a quantitative analysis of the ultrafast dynamics, we report in Fig. 2c the fit to the $\delta R(\omega, t)/R$ spectra at fixed delays ($t=50, 100, 200, 600$ fs), from which we can extract the time evolution of the CT redshift ($\delta\Delta_{CT}$). For all the underdoped samples, the $\delta\Delta_{CT}$ dynamics (see Fig. 2d) is similar and is characterized by two exponential recovery times, $\tau_1=100\pm$ fs and $\tau_2=600\pm$ fs. These timescales are compatible with the coupling to the optical buckling and breathing phonons and, subsequently, to the rest of the lattice vibrations[29], while the coupling of the local charge excitations to short-range antiferromagnetic fluctuations is expected to be effective on the 10 fs timescale[30]. The maximum $\delta\Delta_{CT}$ is estimated by considering the value extracted from the fitting procedure at $t=50$ fs. Considering the $p=0.12$ sample, we obtain $\delta\Delta_{CT}=5\pm 1$ meV at the excitation density of 7 J/cm³. The maximum value of the CT redshift, i.e., $\delta\Delta_{CT}=10\pm 2$ meV, is measured at $p=0.10$ hole doping and with the same excitation density.

The measured CT redshift discloses important information about the nature of the charge-transfer transition. This process can be easily rationalized starting from the CT insulator ($p=0$), in which the completely localized picture provides a good description of the fundamental electronic excitations. In this framework, the energy necessary to move a localized hole from the Cu- $3d_{x^2-y^2}$ to the O- $2p_{x,y}$ orbitals is renormalized by the Coulomb *interatomic* potential (U_{pd}) between the excess Cu- $3d$ electron and the holes residing on the nearest neighbouring oxygen sites. In simple terms, U_{pd} provides a binding mechanism for the local Cu- $3d_{x^2-y^2}$ -O- $2p_{x,y}$ exciton. Within this local picture, we can sit on a spin-up polarized Cu atom (see Fig. 1a) and assume that the effect of the pump pulse is to transfer to that atom a fraction of spin-down electrons, $\delta\epsilon_{\downarrow}$, from the oxygens within the same CuO₂ cell. The excess of positive charges on the oxygen atoms leads to an increase of the binding energy of the additional excitons that can be photoinjected on the neighbouring cells by the following probe pulse. This process can be revealed as a decrease of the effective CT energy measured by the probe. Quantitatively, the pump-induced redshift of Δ_{CT} can be estimated by a simple mean field calculation (see Methods):

$$\delta\Delta_{CT} = -\left(2U_{pd} - \frac{5}{24}U_{pp}\right)|\delta\epsilon_{\downarrow}|, \quad (1)$$

where U_{pp} is the Coulomb repulsion between two charges occupying the same O- $2p$ orbital. From a theoretical point of view, the qualitative discussion above strongly suggests that a crucial ingredient to explain the redshift of the charge-transfer gap is the sizable Coulomb interaction, U_{pd} , between neighboring copper and oxygen atoms[31], which is often neglected in theoretical studies of the cuprates. Considering the realistic values $U_{pp} \sim 5$ eV and $U_{pd} \sim 2$ eV and the photodoping $\delta\epsilon_{\downarrow} \sim 0.3\%$ (see Methods), we estimate $\delta\Delta_{CT} \sim 9$ meV, which is in very good quantitative agreement with the measured pump-induced redshift in underdoped samples.

Interestingly, the $\delta\Delta_{CT}$ measured in the experiments progressively decreases as the hole doping increases, until the $p_{cr} \simeq 0.16$ critical doping concentration is reached. The $\delta R(\omega, t)/R$ signal measured on the optimally ($p=0.16$) and over-doped ($p=0.18$) samples does not show any evidence of a CT redshift, while it can be easily reproduced by assuming an average increase of the electron-boson scattering in the Drude component of the dielectric function, in agreement with the results reported in Refs. 29, 30. The picture emerging from these results can be summarized as follows: for $p < p_{cr}$, the photoexcitation induces a redshift of the CT transition, which is qualitatively similar to what expected for a CT insulator[32, 33]; for $p > p_{cr}$ the ultrafast dynamics can be explained by an increase of the scattering rate of the charge carriers, as expected for a metal. The simplest picture is that p_{cr} discriminates, already at high temperature, an underdoped region in which the electronic properties are dominated by the Coulomb interaction between localized Cu- $3d$ and O- $2p$ wavefunctions, from an overdoped region in which the CT excitation involves wavefunctions spread over many sites. We note that this localized-delocalized transition of the CT excitation is clearly distinct from the onset of the pseudogap physics, which evolves from $T \sim 250$ K at very low doping to $T \sim 150$ K at $p=0.16$ and $T \sim 50$ K at $p=0.2$, as observed by Knight-shift measurements[34]. A similar $T^*(p)$ line has been recently observed by monitoring the p - T dependence of the scattering rate of the Drude peak via non-equilibrium infrared spectroscopy in the 0.5-2 eV energy range[35]. Notably, no transition at p_{cr} is observed when we analyse the $\delta R(\omega)/R$ traces extracted at $t > 600$ fs (Fig. 2c), i.e., when the excess energy is dissipated in low-energy excitations and converted into heat. This demonstrates that the effect reported here for doped cuprates remains inaccessible to

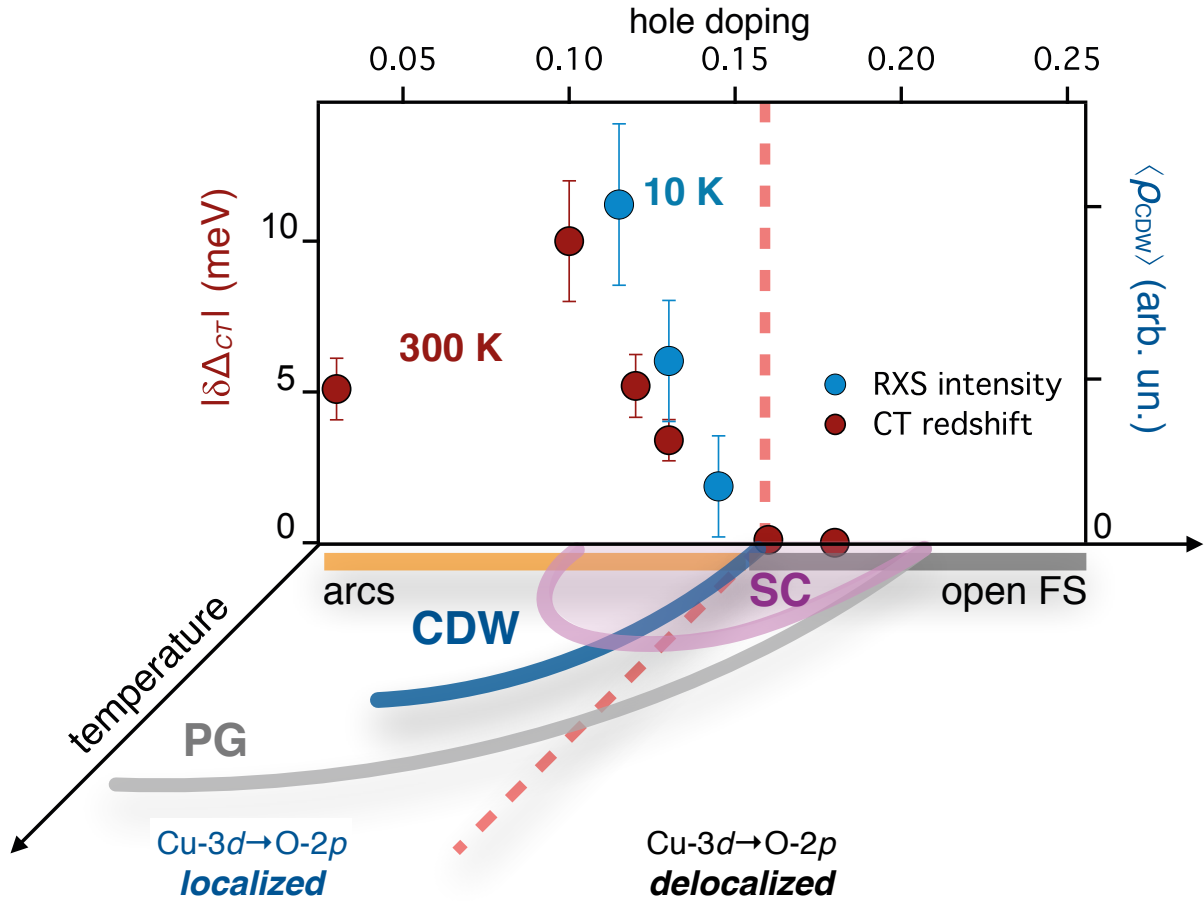


FIG. 3: **The phase diagram of cuprates.** The values of the room-temperature CT redshift ($\delta\Delta_{CT}$, red dots) and the intensity of the low-temperature CDW signal ($\langle\rho_{CDW}\rangle$, blue dots) are reported as a function of the hole concentration of the La-Bi2201 samples. The excitation fluence of the pump beam has been tuned in order to maintain a constant absorbed energy density of 7 J/cm^3 for the different dopings (see Supplementary). $\langle\rho_{CDW}\rangle$ has been obtained by integrating the difference between the RXS signals measured at the temperatures of 10 K and 300 K and at the CDW wavevector [10]. The result has been normalized to the total RXS signal at 300 K. Both $\delta\Delta_{CT}$ and $\langle\rho_{CDW}\rangle$ vanish at the critical doping $p_{cr}=0.16\pm 0.01$, that corresponds to the doping at which a low-temperature transition from Fermi arcs to a closed Fermi surface has been measured by STM[17]. The horizontal (in perspective) panel displays a sketch of the equilibrium p - T phase diagram of copper oxides. The pink, grey and blue lines delimit the superconducting (SC) dome, the pseudogap (PG) and the charge-ordered (CDW) state, respectively.

equilibrium techniques, in which only the charge-fluctuations at $k_B T$ are activated.

We now elucidate the relation between the high-temperature localization of the Cu–O wavefunctions and the low-temperature CDW instability by comparing the results of the ultrafast spectroscopy to the outcome of resonant soft X-ray scattering at $T=10 \text{ K}$ on the same samples[10]. The spontaneous breaking of the translational symmetry of the charge distribution within the CuO_2 planes is detected as a resonance in the RXS signal at a specific exchanged parallel wavevector (see Supplementary). While the width of the RXS peaks indicates a CDW correlation length of the order of 2-3 nm, the momentum-integrated signal can be taken as proportional to the average amplitude of the charge-density modulation. Fig. 3 reports the CDW amplitude, $\langle\rho_{CDW}\rangle$, on La-Bi2201 at different hole doping concentrations, obtained by integrating the RXS signal measured at the proper CDW wavevector. The CDW amplitude progressively decreases until $\langle\rho_{CDW}\rangle \rightarrow 0$ at $p_{cr}=0.16\pm 0.01$, that is the same doping concentration at which the $\delta\Delta_{CT}$ signal vanishes. This observation undoubtedly demonstrates that the development of short-range CDW at low temperature takes place only in the doping region $p < p_{cr}$, that is characterized, already at room temperature, by the intra-unit cell localization of the Cu-3d and O-2p wavefunctions.

The key novelty of these results is the direct link between the room-temperature ultrafast CT dynamics and the low-temperature CDW instability on one single cuprate material. Although further investigation is needed to clarify the nature of the many-body localized Cu–O wavefunctions in terms of the relation, for example, with the physics of the Zhang-Rice singlet and the spin-phonon background, our observations impact on many aspects of the physics of copper oxides: i) charge-order emerges as the low-energy manifestation of a correlated state dominated by the local Cu-3*d*–O-2*p* interactions, whose nature changes at p_{cr} ; ii) the quenching of the O-2*p*→Cu-3*d* charge fluctuations at the energy scale Δ_{CT} plays a relevant role in the charge-ordering phenomenon for $p < p_{cr}$ hole concentrations; iii) the oxygen orbitals are strongly involved in the development of the charge-ordering patterns [4, 23, 36]; iv) the single band Hubbard model turns out to be inadequate to explain the measured $\delta\Delta_{CT}$ (see Methods).

More in general, we note that the critical doping p_{cr} , which is very close to the optimal doping concentration for superconductivity, is a turning point for many low-temperature properties of copper oxides, such as the momentum space topology[16, 17], the ARPES quasiparticle strength[37], the superconductivity-induced kinetic energy change[38, 39], the time-reversal symmetry breaking[40] and the change of the in-plane resistivity curvature[41]. All these evidences suggested the existence of a zero-temperature quantum critical point (QCP) at $p \sim p_{cr}$, as recently supported by magnetic quantum oscillations which unveiled in $\text{YBa}_2\text{Cu}_3\text{O}_{6+\delta}$ a strong increase of the quasiparticle effective mass when superconductivity is suppressed by 90 T magnetic fields[42]. In this framework, our results suggest a novel intriguing scenario, in which a high-energy phenomenon at $p=p_{cr}$ is precursor to the development of a genuine low-energy symmetry breaking at the $T=0$ QCP.

Acknowledgements

We thank F. Cilento, G. Coslovich, D. Fausti, F. Parmigiani, D. Mihailovic, P. Prelovsek, U. Bovensiepen, A. Avella, M. Berciu, J. Bonca, A. Chubukov for useful and fruitful discussions. The research activities of S.P., N.M., F.B, G.F., M.F., M.C. and C.G. received funding from the European Union, Seventh Framework Programme (FP7 2007-2013), under Grant No. 280555 (GO FAST). S.D.C. received financial support from Futuro in Ricerca grant No. RBF12SW0J of the Italian Ministry of Education, University and Research. D.B. acknowledges support from the Deutsche Forschungsgemeinschaft (DFG) through the Emmy Noether Program and the EC through the Marie Curie CIG project no. 334463. The work at UBC was supported by the Max Planck-UBC Centre for Quantum Materials, the Killam, A. P. Sloan, Alexander von Humboldt, and NSERC’s Steacie Memorial Fellowships (A.D.), the Canada Research Chairs Program (A.D.), NSERC, CFI, and CIFAR Quantum Materials. M.C. is financed by the European Research Council through FP7/ERC Starting Grant SUPERBAD, Grant Agreement 240524. G.C. acknowledges support by the EC under Graphene Flagship (contract no. CNECT-ICT-604391).

Methods

A. Experiments

A Ti:sapphire amplifier (Clark-MXR model CPA-1) delivers a train of pulses at 1 kHz repetition rate with 150-fs duration at 780 nm central wavelength and is used to simultaneously drive two Non-collinear Optical Parametric Amplifiers (NOPAs) operating in different frequency intervals. All NOPAs are seeded by white light continuum (WLC) generated in a sapphire plate. The first NOPA (NOPA1) is pumped by the second harmonic and amplifies in a beta-barium borate (BBO) crystal pulses with a spectral content between 820 nm (1.5 eV) and 1050 nm (1.2 eV), which are compressed to nearly TL 13-fs duration by a couple of fused silica prisms. This NOPA serves to trigger the dynamics and it is synchronized with a second NOPA (NOPA2), pumped by the second harmonic and using BBO, which is used to probe the reflectivity variation of the system. The spectrum of NOPA2 spans a frequency range between 510 nm (2.4 eV) and 700 nm (1.8 eV) and it is compressed to 7 fs duration by multiple bounces on a pair of chirped mirrors, making the overall temporal resolution of the pump-probe setup below 19 fs. The time delay between pump and probe is adjusted by a motorized delay stage and both the beams are focused on the sample by a spherical mirror in a quasi-collinear geometry. The spectrum of the NOPA2 is detected by a Si spectrometer working at the full 1 kHz laser repetition rate. By recording the reflected probe spectrum at different temporal delays t with and without pump excitation, we measure the differential reflectivity: $\delta R(\omega, t)/R(\omega)=[R(\omega, t)-R_{eq}(\omega)]/R_{eq}(\omega)$. The pump fluence used for the experiments is $500 \mu\text{J}/\text{cm}^2$. The density of CT excitations can be estimated starting from the pump penetration length (l_{pen}) at a specific doping (see Supplementary). For example, assuming $l_{pen} \sim 700$ nm for $\hbar\omega=1.4$ eV and $p=0.10$ we obtain an absorbed energy of $\sim 7 \text{ J}/\text{cm}^3$, which corresponds to a density of $\Delta_{CT}=2$ eV excitations of about $2 \times 10^{19} \text{ cm}^{-3}$. Considering that the density of Cu atoms is $\sim 6 \times 10^{21} \text{ cm}^{-3}$, we obtain that

the fraction of holes transferred from the Cu atoms is $\delta\epsilon_{\downarrow} \sim 3 \times 10^{-3}$. The La-Bi2201 crystals were grown using the floating-zone technique, and characterized as described in Ref. 43.

B. Mean-field calculation of the CT redshift

In the fully atomic picture (half-filling), the hamiltonian governing the physics of the CuO_2 plane can be written as:

$$H = \epsilon_{\text{Cu}} n_d + \epsilon_{\text{O}} (n_{\text{O}_1} + n_{\text{O}_2}) + \frac{U_{dd}}{2} (n_d - 1)^2 + \frac{U_{pp}}{2} \sum_{i=1,2} (n_{\text{O}_i} - 6)^2 + U_{pd} (n_d - 1) \sum_{i=1,2} (n_{\text{O}_i} - 6)$$

in order to minimize the interaction when one electron sits on the Cu atom and both the oxygens (labeled by i) are fully occupied, i.e., $\langle n_d + n_{\text{O}_1} + n_{\text{O}_2} \rangle = 13$. As a crude approximation, we assume a localized spin (up) on the Cu atom through the following parametrization: $\langle n_{d\uparrow} \rangle = 1 - \epsilon_{\uparrow}$, $\langle n_{d\downarrow} \rangle = -\epsilon_{\downarrow}$, and $\langle n_{\text{O}_1\uparrow(\downarrow)} \rangle = \langle n_{\text{O}_2\uparrow(\downarrow)} \rangle = 3 + \frac{\epsilon}{2}$, where $2\epsilon = \epsilon_{\uparrow} + \epsilon_{\downarrow}$ is the total photoinduced change of the occupation of the Cu_{\uparrow} and Cu_{\downarrow} sites.

The mean-field calculation of the mean value of the Cu and O levels, i.e., $\mu_{\text{Cu},\sigma}$ and $\mu_{\text{O},\sigma}$, result to be:

$$\begin{aligned} \mu_{\text{Cu},\uparrow(\downarrow)} &= \epsilon_{\text{Cu}} - U_{dd} (\epsilon_{\downarrow(\uparrow)} + (-)1/2) + 2U_{pd}\epsilon \\ \mu_{\text{O}} &= \epsilon_{\text{O}} + \frac{5}{24} U_{pp} \left(2\epsilon - \frac{72}{5} \right) - 2U_{pd}\epsilon. \end{aligned}$$

In the simplest case of a single band model, the difference between the empty and occupied Cu levels, i.e., $\mu_{\text{Cu},\downarrow} - \mu_{\text{Cu},\uparrow} = U_{dd}$, results independent of the photoinduced occupation, since intrinsically $\epsilon_{\uparrow} = \epsilon_{\downarrow}$. This result suggests that in the single-band Mott insulator, the density of states of the upper- (UHB) and lower-Hubbard bands (LHB) decreases upon photoexcitation, while the gap value remains constant.

The scenario is qualitatively different for a charge-transfer insulator, in which the electrons are transferred from the Cu to the O atoms and the $\epsilon_{\uparrow} = \epsilon_{\downarrow}$ symmetry is broken. If we sit on the spin up Cu site, the effect of the pump excitation is to transfer a certain amount of electrons from the oxygen to the Cu spin down state, i.e., $\delta\epsilon_{\downarrow} < 0$ while $\delta\epsilon_{\uparrow} = 0$. Therefore, the change of the charge-transfer gap measured by the probe pulse is given by:

$$\delta(\mu_{\text{Cu},\downarrow} - \mu_{\text{O}}) = - \left(2U_{pd} - \frac{5}{24} U_{pp} \right) |\delta\epsilon_{\downarrow}|, \quad (2)$$

-
- [1] V. Hinkov, P. Bourges, S. Pailhes, Y. Sidis, A. Ivanov, C. D. Frost, T. G. Perring, C. T. Lin, D. P. Chen, and B. Keimer, *Nat Phys* **3**, 780 (2007), ISSN 1745-2473.
- [2] J. M. Tranquada, G. D. Gu, M. Hücker, Q. Jie, H.-J. Kang, R. Klingeler, Q. Li, N. Tristan, J. S. Wen, G. Y. Xu, et al., *Phys. Rev. B* **78**, 174529 (2008).
- [3] M. v. Zimmermann, A. Vigliante, T. Niemöller, N. Ichikawa, T. Frello, J. Madsen, P. Wochner, S. Uchida, N. H. Andersen, J. M. Tranquada, et al., *EPL* **41**, 629 (1998).
- [4] M. J. Lawler, K. Fujita, J. Lee, a. R. Schmidt, Y. Kohsaka, C. K. Kim, H. Eisaki, S. Uchida, J. C. Davis, J. P. Sethna, et al., *Nature* **466**, 347 (2010), ISSN 1476-4687.
- [5] Y. Li, V. Balédent, G. Yu, N. Barišić, K. Hradil, R. a. Mole, Y. Sidis, P. Steffens, X. Zhao, P. Bourges, et al., *Nature* **468**, 283 (2010), ISSN 1476-4687.
- [6] H. Karapetyan, M. Hücker, G. D. Gu, J. M. Tranquada, M. M. Fejer, J. Xia, and A. Kapitulnik, *Phys. Rev. Lett.* **109**, 147001 (2012).
- [7] A. J. Achkar, R. Sutarto, X. Mao, F. He, A. Frano, S. Blanco-Canosa, M. Le Tacon, G. Ghiringhelli, L. Braicovich, M. Minola, et al., *Phys. Rev. Lett.* **109**, 167001 (2012).
- [8] S. Blanco-Canosa, A. Frano, E. Schierle, J. Porras, T. Loew, M. Minola, M. Bluschke, E. Weschke, B. Keimer, and M. Le Tacon, *Phys. Rev. B* **90**, 054513 (2014).
- [9] J. Chang, E. Blackburn, A. T. Holmes, N. B. Christensen, J. Larsen, J. Mesot, R. Liang, D. A. Bonn, W. N. Hardy, A. Watenphul, et al., *Nat. Phys.* **8**, 871 (2012).
- [10] R. Comin, a. Frano, M. M. Yee, Y. Yoshida, H. Eisaki, E. Schierle, E. Weschke, R. Sutarto, F. He, a. Soumyanarayanan, et al., *Science* **343**, 390 (2014), ISSN 1095-9203.

- [11] R. Comin, R. Sutarto, E. da Silva Neto, L. Chauviere, R. Liang, W. Hardy, D. Bonn, F. He, G. Sawatzky, and A. Damascelli, *Science* **347**, 1335 (2015).
- [12] E. H. da Silva Neto, P. Aynajian, A. Frano, R. Comin, E. Schierle, E. Weschke, A. Gyenis, J. Wen, J. Schneeloch, Z. Xu, et al., *Science* **343**, 393 (2014), ISSN 1095-9203.
- [13] E. H. da Silva Neto, R. Comin, F. He, R. Sutarto, Y. Jiang, R. L. Greene, G. A. Sawatzky, and A. Damascelli, *Science* **347**, 282 (2015).
- [14] G. Ghiringhelli, M. Le Tacon, M. Minola, S. Blanco-Canosa, C. Mazzoli, N. B. Brookes, G. M. De Luca, A. Frano, D. G. Hawthorn, F. He, et al., *Science* **337**, 821 (2012).
- [15] W. Tabis, Y. Li, M. L. Tacon, L. Braicovich, A. Kreyssig, M. Minola, G. Dellea, E. Weschke, M. J. Veit, M. Ramazanoglu, et al., *Nat. Commun.* **5**, 5875 (2014).
- [16] K. Fujita, C. K. Kim, I. Lee, J. Lee, M. H. Hamidian, I. a. Firmo, S. Mukhopadhyay, H. Eisaki, S. Uchida, M. J. Lawler, et al., *Science* **344**, 612 (2014).
- [17] Y. He, Y. Yin, M. Zech, A. Soumyanarayanan, M. M. Yee, T. Williams, M. C. Boyer, K. Chatterjee, W. D. Wise, I. Zeljkovic, et al., *Science* **344**, 608 (2014), ISSN 1095-9203.
- [18] Wang, Y., Agterberg, D.F., and Chubukov, A. et al. Coexistence of charge-density-wave and pair-density-wave orders in underdoped cuprates. arXiv:1501.07287 (2015).
- [19] A. Allais, J. Bauer, and S. Sachdev, *Phys. Rev. B* **90**, 155114 (2014).
- [20] M. A. Metlitski and S. Sachdev, *Phys. Rev. B* **82**, 075128 (2010).
- [21] S. Sachdev and R. La Placa, *Phys. Rev. Lett.* **111**, 027202 (2013).
- [22] Y. Wang and A. Chubukov, *Phys. Rev. B* **90**, 035149 (2014).
- [23] R. Comin, R. Sutarto, F. He, E. H. da Silva Neto, L. Chauviere, A. Frano, R. Liang, W. N. Hardy, D. A. Bonn, Y. Yoshida, et al., *Nat. Mater.* p. Advanced Online Publication. DOI: 10.1038/NMAT4295 (2015), ISSN 1476-4660.
- [24] K. Fujita, M. H. Hamidian, S. D. Edkins, C. K. Kim, Y. Kohsaka, M. Azuma, M. Takano, H. Takagi, H. Eisaki, S.-i. Uchida, et al., *Proceedings of the National Academy of Sciences* **111**, E3026 (2014).
- [25] Chowdhury, D. and Sachdev, S. The enigma of the pseudogap phase of the cuprate superconductors. arXiv:1501.00002 (2014).
- [26] S. Uchida, T. Ido, H. Takagi, T. Arima, Y. Tokura, and S. Tajima, *Phys. Rev. B* **43**, 7942 (1991).
- [27] S. Lupi, D. Nicoletti, O. Limaj, L. Baldassarre, M. Ortolani, S. Ono, Y. Ando, and P. Calvani, *Phys. Rev. Lett.* **102**, 206409 (2009).
- [28] D. Nicoletti, O. Limaj, P. Calvani, G. Rohringer, A. Toschi, G. Sangiovanni, M. Capone, K. Held, S. Ono, Y. Ando, et al., *Phys. Rev. Lett.* **105**, 077002 (2010).
- [29] S. Dal Conte, C. Giannetti, G. Coslovich, F. Cilento, D. Bossini, T. Abebaw, F. Banfi, G. Ferrini, H. Eisaki, M. Greven, et al., *Science* **335**, 1600 (2012).
- [30] S. Dal Conte, L. Vidmar, D. Golez, M. Mierzejewski, G. Soavi, S. Peli, F. Banfi, G. Ferrini, R. Comin, B. M. Ludbrook, et al., *Nature Physics* **11**, 421 (2015), ISSN 1745-2481.
- [31] P. Hansmann, N. Parragh, A. Toschi, G. Sangiovanni, and K. Held, *New Journal of Physics* **16**, 033009 (2014).
- [32] J. P. Falck, A. Levy, M. A. Kastner, and R. J. Birgeneau, *Phys. Rev. Lett.* **69**, 1109 (1992).
- [33] F. Novelli, G. De Filippis, V. Cataudella, M. Esposito, I. Vergara, F. Cilento, E. Sindici, A. Amaricci, C. Giannetti, D. Prabhakaran, et al., *Nat. Commun.* **5**, 5112 (2014).
- [34] S. Kawasaki, C. Lin, P. L. Kuhns, A. P. Reyes, and G.-q. Zheng, *Phys. Rev. Lett.* **105**, 137002 (2010).
- [35] F. Cilento, S. Dal Conte, G. Coslovich, S. Peli, N. Nembrini, S. Mor, F. Banfi, G. Ferrini, H. Eisaki, M. K. Chan, et al., *Nature Communications* **5**, 4353 (2014).
- [36] J. Zaanen, G. Sawatzky, and J. Allen, *Phys. Rev. Lett.* **55**, 418 (1985).
- [37] D. Fournier, G. Levy, Y. Pennec, J. L. McChesney, a. Bostwick, E. Rotenberg, R. Liang, W. N. Hardy, D. a. Bonn, I. S. Elfimov, et al., *Nature Physics* **6**, 905 (2010).
- [38] G. Deutscher, A. F. Santander-Syro, and N. Bontemps, *Phys. Rev. B* **72**, 092504 (2005).
- [39] C. Giannetti, F. Cilento, S. Dal Conte, G. Coslovich, G. Ferrini, H. Molegraaf, M. Raichle, R. Liang, H. Eisaki, M. Greven, et al., *Nat. Comm.* **2**, 353 (2011).
- [40] J. Xia, E. Schemm, G. Deutscher, S. A. Kivelson, D. A. Bonn, W. N. Hardy, R. Liang, W. Siemons, G. Koster, M. M. Fejer, et al., *Phys. Rev. Lett.* **100**, 127002 (2008).
- [41] Y. Ando, S. Komiya, K. Segawa, S. Ono, and Y. Kurita, *Phys. Rev. Lett.* **93**, 267001 (2004).
- [42] B. J. Ramshaw, S. E. Sebastian, R. D. McDonald, J. Day, B. S. Tan, Z. Zhu, J. B. Betts, R. Liang, D. A. Bonn, W. N. Hardy, et al., *Science* **348**, 317 (2015).
- [43] S. Ono and Y. Ando, *Phys. Rev. B* **67**, 104512 (2003).
- [44] Y. S. Lee, K. Segawa, Z. Q. Li, W. J. Padilla, M. Dumm, S. V. Dordevic, C. C. Homes, Y. Ando, and D. N. Basov, *Phys. Rev. B* **72**, 054529 (2005).

Supplementary Materials

Optical Properties of $\text{Bi}_2\text{Sr}_{2-x}\text{La}_x\text{CuO}_{6+\delta}$ at equilibrium

In Figure S4 we report the light penetration depth in La-Bi2201, as a function of the photon energy at different doping concentrations. The penetration depth (d_{pen}) has been obtained from the La-Bi2212 optical conductivity that has been measured elsewhere [27]. Since the density of the CT excitations induced by the pump pulse depends on the energy density delivered by the pump pulse, the knowledge of d_{pen} is necessary to maintain a constant excitation density when the doping is changed. At the pump photon energy of 1.4 eV, d_{pen} decreases as the doping is increased, as shown in Figure S4. This is the consequence of the progressive increase of the charge carrier density which results in a larger Drude contribution to the absorption process. The incident fluence has been tuned in order to maintain a constant excitation density of 7 J/cm^3 for all the time-resolved measurements at different doping concentrations.

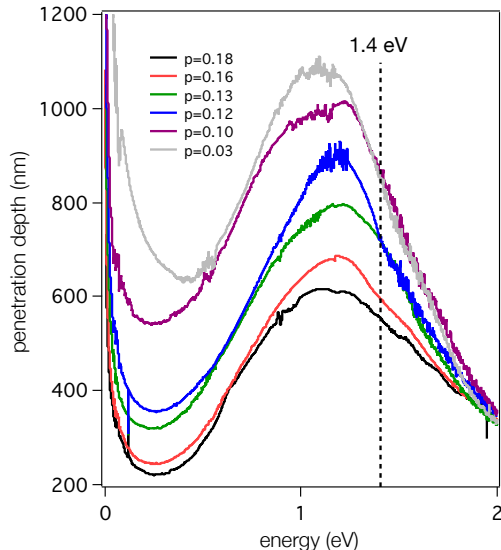


FIG. 4: Light penetration depth in $\text{Bi}_2\text{Sr}_{2-x}\text{La}_x\text{CuO}_{6+\delta}$, as a function of the photon energy and for different doping concentrations, $0.03 < p < 0.18$. The photon energy of the pump pulse (1.4 eV) is indicated by a black dashed line.

Ultrafast reflectivity variation in the UV-vis spectral range

In order to rule out the possibility that, in optimally and over-doped La-Bi2201 samples, the absence of the CT redshift is related to a substantial increase of the Δ_{CT} energy, which would push the observed phenomenon out of the explored energy window, we extended the time-resolved measurements up to an energy of 3 eV. In this case the pump beam is the output of a visible NOPA (see methods) while the probe beam is generated by non-linear optical processes in a 2mm thick CaF_2 crystal. In Figure S5 we report the $\delta R(\omega, t)/R$ matrix measured on the overdoped La-Bi2201 sample ($p=0.18$). The absence of any negative component in the signal, allows us to conclude that no CT redshift is observed in the energy range that extends far above the Δ_{CT} energy estimated by equilibrium optical spectroscopy. The same experiment has been repeated at different pump photon energies ($\hbar\omega = 2.06 \text{ eV}$ and $\hbar\omega = 1.77 \text{ eV}$). The measured dynamics did not evidence any significant change, in agreement with the results reported in the main text.

Differential analysis of the transient reflectivity variation induced by changes in the equilibrium dielectric function

The analysis of the time-resolved data has been carried out starting from the equilibrium dielectric function of the samples which has been measured elsewhere [27]. The best fitting to the complex optical conductivity has been

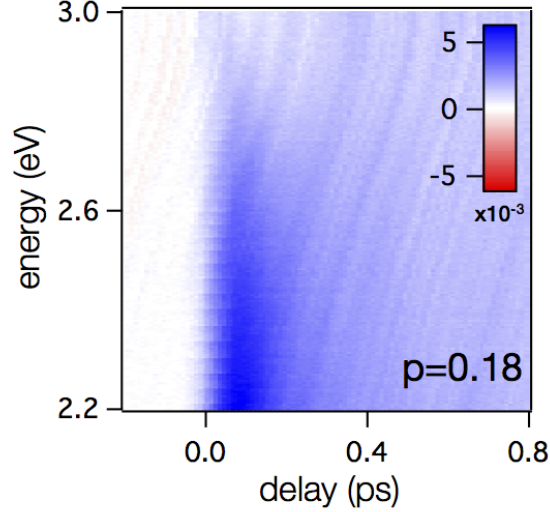


FIG. 5: Ultrafast reflectivity variation, $\delta R(\omega, t)/R$, measured by optical spectroscopy on the $p=0.18$ La-Bi2201 sample. The pump photon energy was set at 2.06 eV. The colour scale is reported in the inset.

obtained by combining a Drude model [29, 30] and various high-energy Lorentz oscillators with the addition of a mid-infrared (MIR) oscillator:

$$\sigma(\omega) = \epsilon_0 \frac{\omega_D^2}{\gamma_D - i\omega} + \epsilon_0 \omega \frac{\omega_{PMIR}^2}{\omega \gamma_{MIR} - i(\omega^2 - \omega_{MIR}^2)} + \epsilon_0 \omega \sum_j \frac{\omega_{pj}^2}{\omega \gamma_j - i(\omega^2 - \omega_j^2)} \quad (3)$$

The first term represents the relaxation of the free charge carriers characterized by the scattering rate γ_D and addresses the low energy excitations; the second term accounts for the ubiquitous MIR peak observed in copper oxides [44], which can be attributed to a transition from the lower Hubbard band to the Fermi level; the third term is a sum of Lorentz oscillators - characterized by the central frequency ω_j , the strength of the oscillator ω_{pj}^2 , and the scattering rate γ_j - that describe the response of bound charges. The first of these oscillator, whose position is centered around 2 eV, is related to the charge-transfer excitation (CT), i.e. the excitations between $Cu-3d$ and $O-2p$ orbitals [26].

The idea of the differential model is to find the minimum number of parameters in the dielectric function which have to be modified to reproduce the reflectivity variation, i.e. $\delta R(\omega, \tau)/R$, measured at a given time delay τ . As discussed in Refs. [29, 30] the $\delta R(\omega, \tau)/R$ signal measured on optimally and overdoped copper oxides can be interpreted, already after ~ 40 fs, as a transient increase of the electron-boson scattering rate. The increase of the γ_D induces a broadening of the Drude plasma edge across the plasma frequency at $\omega_D \sim 1$ eV. The $\delta R(\omega, \tau)/R$ detected at probe frequencies $\omega > \omega_D$ results in a positive and featureless signal, which monotonically decreases at large frequencies. This behaviour, that is confirmed in the measurements on La-Bi2201 for hole concentrations $p \geq 0.16$, clearly contrasts with the $\delta R(\omega, \tau)/R$ signal observed at $p < 0.16$ and for $\tau \lesssim 600$ fs (see Fig. 2 of the main manuscript). As an example, we report in Fig. S6 the signal $\delta R(\omega, \tau = 50 \text{ fs})/R$ measured on the underdoped La-Bi2201 sample with $p=0.12$. Clearly, the negative reflectivity variation at $\omega > \Delta_{CT} \simeq 2$ eV cannot be attributed to a change of the electron-boson scattering rate (dashed green line, SR). On the other hand, the $\delta R(\omega, \tau)/R$ signal is perfectly reproduced simply by assuming a redshift of the CT oscillator (dashed blue line, RS) alone. For completeness, we also show that a change in the spectral weight of the CT oscillator (dashed red line, SW) does not account for the measured $\delta R(\omega, \tau)/R$.

Resonant soft X-ray scattering (RXS) on $\text{Bi}_2\text{Sr}_{2-x}\text{La}_x\text{CuO}_{6+\delta}$

In Fig. S7 we show resonant soft X-ray scattering (RXS) measurements on $\text{Bi}_2\text{Sr}_{2-x}\text{La}_x\text{CuO}_{6+\delta}$ at the $\text{Cu-}L_3$ edge. The RXS signal, $I(q_{\parallel})$, measured at $T=10$ K is reported as a function of the in-plane exchanged momentum (q_{\parallel}) for three different doping concentrations, i.e., $p=0.10, 0.13, 0.15$. We use the common notation for q_{\parallel} , in which the reciprocal lattice units (r.l.u.) for the momentum axes are defined as $2\pi/a_0=1$, where $a_0=3.86 \text{ \AA}$ is the length of the primitive vectors of the tetragonal crystallographic \mathbf{a} and \mathbf{b} axes.

The resonances in the $I(q_{\parallel})$ signal at $q_{\parallel} \sim 0.27$ evidence the presence of a spontaneous inhomogeneous charge distribution within the CuO_2 planes, which breaks the translational symmetry. The resonance disappears when the

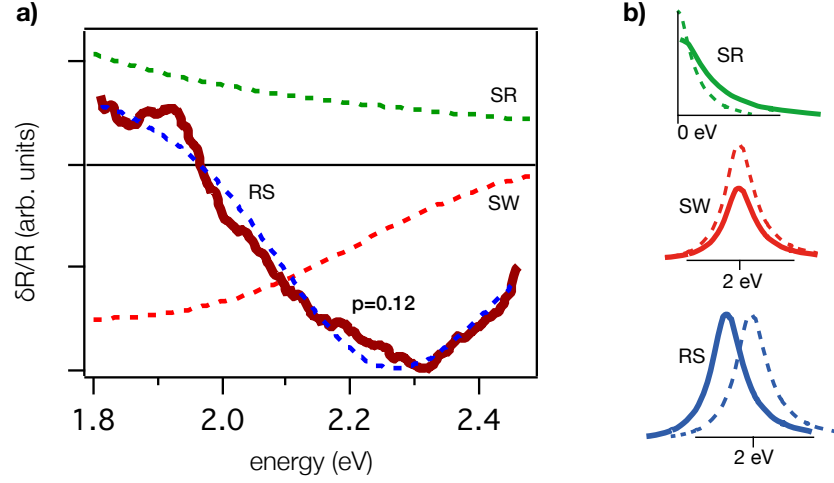


FIG. 6: a) $\delta R(\omega, \tau)/R$ (purple solid line) measured on the $p=0.12$ La-Bi2201 sample at a delay $\tau=50$ fs. The dashed lines are the reflectivity variations calculated by modifying different parameters in the equilibrium dielectric function. In particular, we considered the increase of the total scattering rate in the Drude part of the optical conductivity (dashed green line, SR), the redshift of Δ_{CT} (dashed blue line, RS) and the change of the CT spectral weight (dashed red line, SW). b) A pictorial view of the modification of the optical conductivity for the three cases is reported.

temperature is increased, as extensively discussed in Ref. 10. The amplitude of the charge density modulation is calculated as:

$$\langle \rho_{CDW} \rangle = \frac{\int_{q_{||}} [I(q_{||}, T = 10K) - I(q_{||}, T = 300K)] dq_{||}}{\int_{q_{||}} I(q_{||}, T = 300K) dq_{||}} \quad (4)$$

The figure S7 has been readapted from Ref. 10.

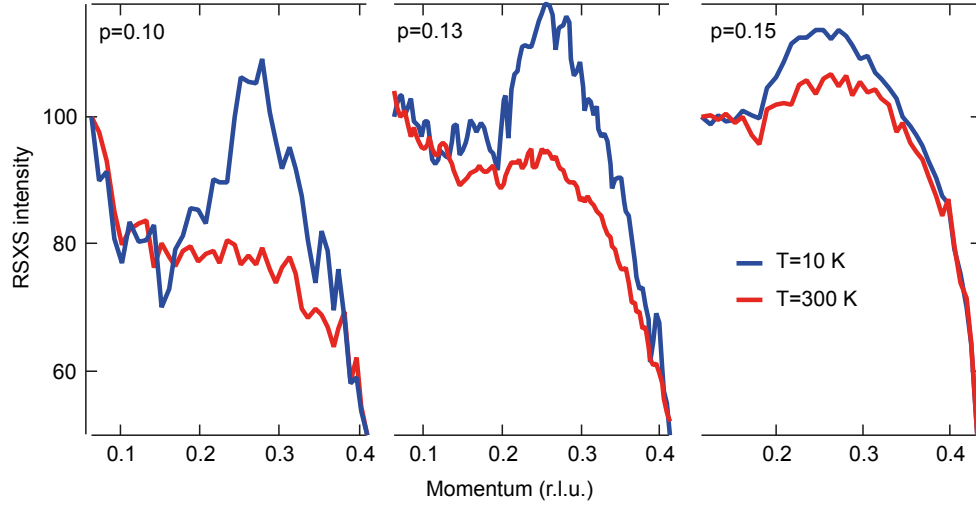


FIG. 7: Low- and high-temperature $I(q_{||})$ signal as measured by RIXS for different doping concentrations. Readapted from Ref. 10.